Is stress modeling able to forecast intrusions and slip events at Piton de la Fournaise volcano ?

Quentin Dumont, Valérie Cayol, Jean-Luc Froger

Highlights

Is stress modeling able to forecast intrusions and slip events at Piton de la Fournaise volcano ?

Dumont Quentin[a], Cayol Valérie[a], Froger Jean-Luc[b]

- We compute stress changes for 60 eruptions that took place from 1998 to 2021.
- Prior to a major eruption in 2007, stress changes have no predictive value.
- After 2007, stress changes agree with the location of intrusion and flank slip.
- A positive feedback between rift intrusions and flank slip events is documented.
- Over a longer timescale, these stress changes favor major flank collapses.

Is stress modeling able to forecast intrusions and slip events at Piton de la Fournaise volcano ?

Dumont Quentin[a]*, Cayol Valérie[a], Froger Jean-Luc[b]

[a] *Université Clermont Auvergne, CNRS, IRD, OPGC, Laboratoire Magmas et Volcans, F-63000 Clermont-Ferrand, France*

[b] *Université Jean Monnet - Faculté des Sciences et Techniques, Laboratoire de géologie de Lyon : Terre, Planètes, Environnement - UMR CNRS 5276 LGL-TPE, 42023 Saint-Etienne, France*

Abstract

Widespread evidence indicates that the stress field and the presence of major discontinuities control the magma trajectory and the stability of volcanic edifices. These latter factors affect two major volcanic hazards: eruptions and flank slip events. Here, we use a catalog of 60 intrusions at Piton de la Fournaise (Réunion Island) to document the link between stress inherited from intrusions and slip events, and the location of subsequent events. Our study spans two periods, 1998-2007 and 2007-2021, separated by a collapse of the summit crater and a 1.4 meter flank slip in 2007. The 1998-2007 intrusive sequence cannot be explained by stress interaction. On the contrary, the location of intrusions in the 2007-2021 sequence is consistent with a decrease in normal stresses (unclamping) induced by previous intrusions. Progressive rift zone unclamping, and Coulomb stress increase on previously recognized structures explain the migration of activity from the summit to distal areas, the alternation between intrusions in the northern and the southern flanks, as well as the occurrence of flank slip events. Stress analysis documents a positive feedback between rift zone and flank slip events. In the long term, both magma intrusions and flank slip events contribute to the occurrence of catastrophic flank collapses through unclamping and Coulomb stress increase at the

*Corresponding author

Email address: quentindumont@live.fr (Dumont Quentin[a])

base of an unstable sector.

Keywords: Ground deformation, Stress field modeling, Normal stress change, Coulomb Stress Change, Flank instability

---

1. Introduction

Two major hazards at basaltic shield volcanoes are rift zone intrusions, which feed lava flows, and flank slip events, which could results in various subsequent hazards (e.g. debris avalanche and landslides; tsunami; earthquakes), impacting infrastructures and causing fatalities (*Auker et al.*, 2013). For instance, at Piton de la Fournaise (Réunion Island, France), one of the major hazards is the propagation of intrusions along the main rift zone beyond the limits of the caldera walls, as this may feed lava flows that travel onto the inhabited flanks of the volcano. The 1977 eruption reached the village of Sainte-Rose on the north flank of the volcano, and the 1986 eruption destroyed eight houses and forced the evacuation of 429 people on the south flank. Now that the island population has increased by 180%, such eruptions threaten more than 11500 people (*Villeneuve and Bachelery*, 2006). The other major hazard is sudden large scale flank displacements. Bathymetric studies around Réunion Island (*Oehler et al.*, 2008) have shown the occurrence of around 50 mass wasting events in the last two million years. Such events may induce large earthquakes, like those triggered at Hawaii in 1975 (M7.2, *Owen and Burgmann*, 2006) and in 2018 (M6.9, *Lin and Okubo*, 2020), as well as tsunami, such as those affecting Réunion and Mauritius islands (*Kelfoun et al.*, 2010). Assessing where these hazards will take place is a major challenge.

Voluminous intrusions and flank slip events are interrelated hazards, the former often co-inciding with the latter. For example, at Kilauea (Hawaii, USA), the 2007 intrusion took place at the same time as a slow slip event (*Montgomery-Brown et al.*, 2015), at Mount Etna (Italy), the December 2018 paroxysmal eruption (*Pezzo et al.*, 2020) triggered a seaward flank slip, and at Piton de la Fournaise, in 2007, the largest historical eruption of the volcano was accompanied by a 1.4 m seaward slip. Mechanical models show that magma intrusions pro-

mote flank slip and conversely that the persistence of rift zones depends on the mobility of the volcano flanks, as demonstrated for Kilauea by *Dieterich* (1988).

Predicting eruptive vents can be based on a probabilistic approach using density maps of previous vents (*Chevrel et al.*, 2021). However, this approach suffers from certain limitations. Firstly, to be reliable, the approach requires a sufficiently long and detailed record of past activity, which might not be available for volcanoes with very little activity. Secondly, this approach is only intended to assess long term volcanic hazards rather than to pinpoint the location of the next eruption. For example, at basaltic shield volcanoes, such as in Hawaii or Réunion Island, where preferential intrusions zones (referred to as rift zones) are clearly identified (*Michon et al.*, 2015), vent density maps highlight rift zones which are tens of kilometers long, while eruptive vents are generally only a kilometer long. While the next eruption would be expected to occur at some point along the rift zones, the exact location is not known.

Because the magma pathway is controlled by the stress field and mechanical properties of the host rock, as well as by the physics of magma transport, an alternative and more reliable approach relies on mechanical and physical modeling. To the first order, magma intrusions, whether dykes or sills, emplace perpendicular to the minimum principal stress (*Anderson*, 1951). Consequently, the characterization of crustal stress and its temporal change can be used to explain (*Buck et al.*, 2006; *Walter and Amelung*, 2006; *Amelung et al.*, 2007) and predict the location of intrusions (*Rivalta et al.*, 2019; *Mantiloni et al.*, 2021). Crustal stress results primarily from the weight of the dense host rock, but also from multiple factors and processes (*Rivalta et al.*, 2015): (1) the extensional or compressional nature of the regional tectonics (*Buck et al.*, 2006; *Menand et al.*, 2010); (2) density and rigidity changes (*Maccaferri et al.*, 2011); (3) edifice load (*Pinel and Jaupart*, 2000) or ocean level changes (*Le Corvec and McGovern*, 2018);(4) caldera collapse (*Corbi et al.*, 2015), lateral flank collapse (*Maccaferri et al.*, 2017) or ice cap retreat (*Albino et al.*, 2010); (5) pressurization/depressurization of the magma chamber or hydrothermal system (*Chadwick and Dieterich*, 1995;

Gudmundsson, 2012); (6) magmatic intrusions (*Buck et al.*, 2006; *Grandin et al.*, 2010); and finally (7) large earthquakes (*Walter and Amelung*, 2006). Apart from stress, other parameters also influence the shape, location and dynamics of magma propagation, as demonstrated by numerical models and laboratory experiments (*Rivalta et al.*, 2015). For instance, preexisting discontinuities, if suitably oriented, may channel intrusions and modify their propagation (*Ruch et al.*, 2016; *Dumont et al.*, 2022). Strength of the host rock, toughness and length of the eruptive fissure, as well as physical properties of the magma (density and viscosity) may influence the shape, propagation direction and velocity of magma intrusions (*Maccaferri et al.*, 2011). The respective influence of these factors remains to be determined.

Here, we track stress changes at major recognized discontinuities on Piton de la Fournaise in order to anticipate the location of magma intrusions and associated vents, as well as the occurrence of flank slip events. We chose to test the approach on Piton de la Fournaise as it is not only one of the most active volcanoes in the world, with 2.5 eruptions per year on average since 1998 (Figure 1a), but it also has one of the densest monitoring networks, making it highly suitable for investigating the parameters that control the location of eruptive vents. Using systematic satellite deformation monitoring (Synthetic aperture radar interferometry, InSAR), which has been carried out here since 1998, we applied inverse modelling to data from 22 years of intrusive activity (*Dumont et al.*, 2022). The intrusion geometries determined by the inversions highlight a main spoon-shaped rift zone, extending beneath the east flank as a sub-horizontal sill intrusion zone and fault. Four secondary rift zones radiating from the summit were also highlighted (Figure 1). We note that these rift zones guide intrusions.

In order to estimate whether stress changes favor intrusions, we computed cumulated changes in normal stress in the previously identified rift zones. To estimate whether intrusions promote flank slip, we also calculated Coulomb stress changes on the sub-horizontal part of the main intrusive structure. In the final part of the paper, we discuss the major processes that might explain the spatio-temporal sequence of intrusions and flank slip events, and their im-

plications for Piton de la Fournaise, with the aim of better assessing the location of future intrusions.

2. Internal structure of Piton de la Fournaise

Piton de la Fournaise is a basaltic shield volcano located in the south-east of Réunion Island (Indian Ocean). To the west, Piton de la Fournaise is buttressed by the extinct Piton des Neiges volcano, while its eastern flank is characterized by steep ocean-ward slopes of up to 35°, and is affected by seaward flank slip. This slip can be sudden, as shown by satellite interferometry during a major eruption in 2007 (*Froger et al.*, 2015), or steady at a rate of 1.4 cm/yr, sometimes showing transient acceleration after rift zone intrusions, as shown by InSAR and continuous global navigation satellite system (GNSS) data (*Peltier et al.*, 2015a; *Chen et al.*, 2017).

The main structural feature of the volcano is a U-shaped caldera of 8 km (N-S) by 13 km (W-E), delimited by steep walls of 100 to 200 m in height (Figure 1). The volcanic center, characterized by a 400 m-high cone with a diameter of 3.4 km, is located within this caldera. There is a 1 km diameter crater (the Dolomieu) at the summit.

Piton de la Fournaise activity is characterized by cycles of intense activity separated by periods of quiescence lasting a few years. Since March 1998, Piton de la Fournaise has experienced two eruptive cycles characterized by a deep magma supply. The first cycle followed a rest-period of 66 months. It started with deep magma ascent in March 1998, evidenced by seismicity (*Battaglia et al.*, 2005) and geochemistry (*Vlastélic et al.*, 2018). Subsequent eruptions alternated between summit ($<$ 1 km from the summit), proximal (between 1 and 2 km from the summit) and distal ($>$ 2 km from the summit) locations (*Peltier et al.*, 2008) up to the March-April 2007 eruption, which is the largest historical eruption. The eruption involved the emission of 220 Mm^3 of lava, a collapse of the Dolomieu crater by 330 m (*Staudacher et al.*, 2009) and a 1.4 m eastward flank slip (*Froger et al.*, 2015). In the three years following the eruption, eruptive activity changed to low-volume summit eruptions and to a

large number of dyke arrests (*Roult et al.*, 2012), before a pause in December 2010 (*Peltier et al.*, 2010). The second cycle started after a 42-month quiescence, in June 2014, after a further ~~phase~~ episode of deep magma transfer evidenced by continuous GNSS data (*Beauducel et al.*, 2020) and geochemistry (*Vlastélic et al.*, 2018) and migration of deep earthquakes in 2015 (*Lengliné et al.*, 2016). Between June 2014 and October 2021, the volcano experienced 22 eruptions and 3 aborted eruptions (intrusions that did not reach the surface). The rate of magma supply remained constant over the 1998-2021 period (Figure 1b), despite the large emitted volume in 2007, and the small emitted volume afterwards from 2008 to 2014. In contrast to these eruptive "cycles" defined mainly by new magma resupply from the depth, and in order not to confuse them with the evolution of the stress field, which is the subject of this study, we will refer to stress field evolution "phases" in the following of this manuscript.

Most eruptions were characterized by the opening of eruptive fissures along a main north-east to south-east rift zone (NERZ-SERZ, see Figure 1) passing through the Dolomieu crater (*Michon et al.*, 2015; *Peltier et al.*, 2015b; *Dumont et al.*, 2022). Typically, as shown by tilt data (*Peltier et al.*, 2005) and joint inversions of InSAR and continuous GNSS data (*Smittarello et al.*, 2019), eruptions started with vertical magma migration beneath the summit crater, followed by a lateral migration towards the vent. This lateral migration sometimes began with sills which became vertical in the NERZ or SERZ (*Smittarello et al.*, 2019; *Dumont et al.*, 2022).

Three main seismicity zones were identified at the volcano (*Duputel et al.*, 2021): (1) A deep seismicity zone below the summit crater, between -5 km and sea level, which was activated during magma resupply from depth in 1998 (*Battaglia et al.*, 2005) and in 2015 (*Lengliné et al.*, 2016); (2) pre-eruptive seismic swarms located between sea-level and 1 km below the summit crater whose activity started days to hours before eruptions and stopped during magma propagation in the rift zone; (3) a seismic trend dipping 40° eastward, and located beneath the eastern flank at depths ranging between 0 and 4 km below sea level (from west

to east).

In a previous study (*Dumont et al.*, 2022) we determined the intrusion geometry of 57 events

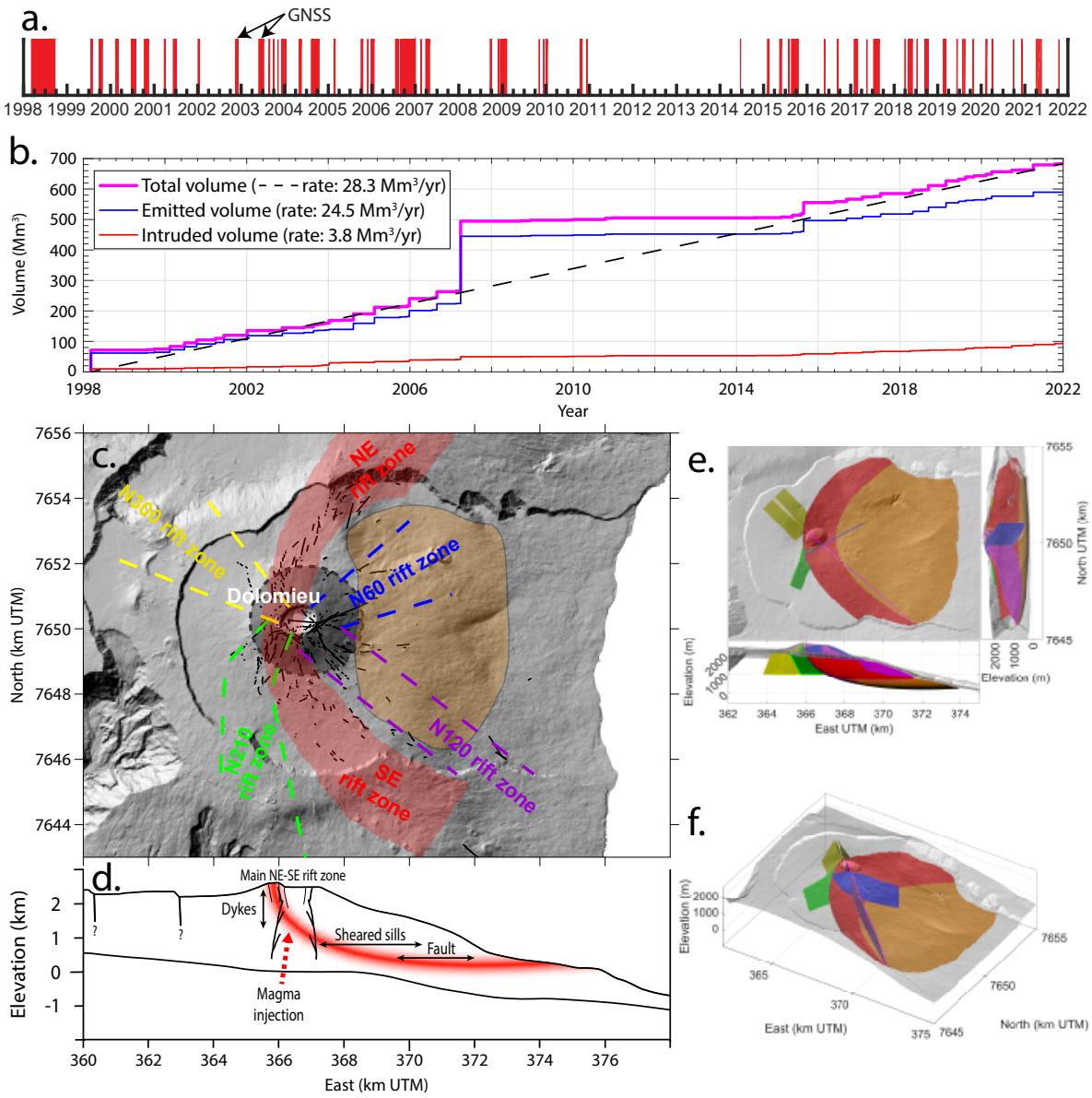

Fig. 1: Piton de la Fournaise intrusions and rift zones. a. Chronology of intrusive events since 1998. Each red band indicates an intrusive event, with the width corresponding to its duration. GNSS data alone was used for the two events indicated by arrows. b. Emitted and intruded cumulated volumes at Piton de la Fournaise for the 1998-2022 period (mean emission rates are also given). c. Main rift-zones of the volcano on a shaded DEM. The main NE-SE rift zone is highlighted by the pale red shaded area, while the N60°, N120°, N210° and N300° rift zones are marked by blue, magenta, green and yellow dashed lines, respectively. Circular dark gray patch indicates the summit cone area. Light orange shading highlights the area affected by eastward slip during the January 2004, April 2007, October 2019, September 2020 and October 2021 intrusions. Black segments indicate historical eruptive fissures. d. West-east cross-section of the main NE-SE rift zone as determined by *Dumont et al.* (2022). e. and f. Map with cross-sections and a perspective view of the idealized rift zone geometries used for stress computations. Rift zones are color-coded with the same colors as in c.

using a method which combines 3D boundary element modelling (*Cayol and Cornet*, 1997, 1998), with Monte Carlo inversions (*Fukushima et al.*, 2005). In contrast to classical dislocation solutions used to study volcano deformation, topography was taken into account, intrusions could be curved, and co-eval normal and shear stress changes on fractures were inverted. From the inversions and the interpolation of 29 intrusions, we highlighted a major arcuate structure connected at the surface to the already recognized NERZ and SERZ (*Dumont et al.*, 2022). This structure is spoon-shaped, with an evolution in dip from sub-vertical at shallow depth to sub-horizontal to the east, at greater depths (500-1000 m above sea level). This structure was shown to be undergoing (1) pure opening at the head of the structure, (2) coeval slip and opening further east, (3) and slip alone in its easternmost part. This spoon-shaped rift zone differs in length and shape from classic rift zones found at larger shield volcanoes or at rift volcanoes. It is smaller in extent (around 10 km), shallower (1 km), and has an along-dip curvature. Typically, rift zones at shield and rift volcanoes, such as Kilauea (*Peltier et al.*, 2015b), Krafla (*Buck et al.*, 2006) and Bardarbunga (*Sigmundsson et al.*, 2015), extend for tens to hundreds of kilometers, can reach a depth of 10 km, and are sub-vertical.

Besides the main NERZ-SERZ, we detected four secondary rift zones (*Dumont et al.*, 2022). Two of them, those with N60° (N60RZ) and N120° (N120RZ) orientations, start at the south-eastern border of the Dolomieu crater (*Michon et al.*, 2015; *Dumont et al.*, 2022). We suggested (*Dumont et al.*, 2022) that these two axes are induced by the NERZ-SERZ, rather than by a crustal structure, as they only accommodate shallow intrusions. The two others, oriented N210° (N210RZ) and N300° (N300RZ), are located to the southwest and northwest of the summit cone but are less well constrained due to being less active (*Michon et al.*, 2015; *Dumont et al.*, 2022).

3. Method

3.1. Method for 3D stress computation

To investigate how previous intrusions affect the location of subsequent intrusions, we computed the stress changes over the course of the 60 intrusions that took place from March 1998 to October 2021. We focused on the accumulated stress, rather than stress associated with the individual event, as InSAR data evidence that deformation accumulates and that stress relaxation is negligible. We computed the stress history of the 1998-2007 and 2007-2021 periods separately. These periods were chosen over the periods corresponding to deep magma supply (1998 to 2014 and 2014-2015 to 2021), as there is evidence that the intrusive behavior of the volcano changed after 2007 (*Peltier et al.*, 2010; and Figure 1b) whereas it did not change after the 2014-2015 deep supply. Intrusive activity is the result of deep magma transfer and stress modulation by deformation of the edifice. Here, intrusive activity shows that supply has a negligible influence on stress in the shallow edifice. We therefore focus on stress modulation caused by both intrusions and fault slip events in the shallow part of the edifice.

We used our previous study (*Dumont et al.*, 2022), which determined the characteristics of each intrusion by inverse modeling of InSAR, or GNSS campaign data when InSAR data were lacking (Figure 1a). For consistency, we computed the 3D stress field induced by each intrusion using the same method (*Cayol and Cornet*, 1997, 1998) as in our previous study (*Dumont et al.*, 2022). Because this study demonstrated that intrusions take place in well-defined rift zones, we computed stress changes induced in these rift zones. Computations assume an elastic, linear and homogeneous medium. Boundaries (intrusions and the ground surface) are meshed by triangular elements, with boundary conditions given by stress. They are null at the ground surface and equal to a homogeneous pressure, or stress vector elsewhere. Mechanical parameters are set to be equal to those used for the inverse modeling of intrusion geometries (*Dumont et al.*, 2022): the Young's modulus is 5 GPa and the Poisson's coefficient is 0.25. These values follow estimations of *Cayol and Cornet* (1998) from seismic velocities at Piton de la Fournaise corrected for the pressure at the intrusion depth. They are

consistent with in-situ measurements by *Heap et al.* (2020) for basaltic volcanoes.

We ignored several time-dependent processes which have negligible influence compared to the stress changes induced by the intrusions and faults. Stress relaxation between eruptions was not taken into consideration as there is no evidence of deformation associated with this process. We also assume that the steady flank slip has a small enough amplitude (1.4 cm/yr) to have a negligible influence on stress. This assumption is validated by the post-eruptive displacement following the March-April 2007 slip event. In one year, 15 cm of eastward and 30 cm of downward displacements were recorded (*Froger et al.*, 2015), which is equivalent to the cumulated steady flank slip for our study period. These displacements only resulted in 0.02 MPa of stress change in the rift zones (see Figure 2 and Supplementary Figure S2). We ignored static stress load from lava flows for the following reason. Each lava flow during the 2014-2018 period averaged 6.5 meters in thickness (*Hrysiewicz*, 2019); considering an average bulk density of 1300 kg/m^3 (Gurioli, personal communication), this led to an average load of 0.08 MPa per lava flow. In addition, since lava flows rarely cover the same area, this influence is not cumulative. Long term pressure changes induced in the magma reservoirs or in the hydrothermal system were not taken into account because the associated signals are weak (*Peltier et al.*, 2015b). Our simulations show they result in a stress decrease of less than 0.03 MPa in the rift zone (see Supplementary Figure S3). Finally, stress changes induced by earthquakes were also ignored as most seismic events at Piton de la Fournaise have a magnitude of less than M_W <1, with only few with a magnitude of M_W 3 (*Duputel et al.*, 2021).

3.2. Cumulated normal and Coulomb stress changes in the rift zones

For each intrusion, 3D stress tensors were computed on a regular grid, with a 50 m spacing. For the sake of computational and visual simplicity, we interpolated the stress tensors onto the previously determined 3D surfaces of the rifts zones (*Dumont et al.*, 2022; Figure 1d-e) using a nearest neighbor interpolation. We then resolved the stress vectors on these rift zones. The NERZ-SERZ represents the upper part of the spoon shaped structure (in red on Figure

1d-e), while the area of sills and slip events corresponds to its lower part (in orange on Figure 1d-e). The N60RZ and N120RZ rift zones were determined to be vertical, but rooted in the main NERZ-SERZ. The N210RZ has a mean dip of 60° eastward. The N300RZ, which has only been determined based on two eruptions, is the least well constrained. Thus, we consider three different dips for stress computations: 60° eastward, 60° westward and purely vertical. All structures are meshed with triangular elements, as for the forward simulation boundaries.

In addition, for statistical purposes, we computed the stress change on the actual geometry of each intrusion within its 95% confidence interval as determined by inverse modeling (*Dumont et al.*, 2022; see Supplementary movies).

To identify those areas where new intrusions would be favored, we looked at the normal stress change amplitude. Because the host rock is in a compressive state of stress, the opening of an intrusion at a given orientation (strike and dip) would be promoted if the normal stress applied to this surface were to decrease, corresponding to a negative normal stress change. Conversely, the opening of an intrusion would be inhibited if the normal stress applied to this surface were to increase, corresponding to a positive normal stress change (*Amelung et al.*, 2007).

To investigate the impact of intrusions on flank stability, in addition to normal stress changes, we computed Coulomb failure stress changes (ΔCFS) on the main spoon-shaped structure. We used the general formulation of Coulomb stress change given by:

$$\Delta CFS = \Delta\tau - \mu'\Delta\sigma_n, \tag{1}$$

where $\Delta\tau$ is the shear stress change in the potential direction of slip, $\Delta\sigma_n$ is the normal stress change and μ' is the effective friction coefficient accounting for changes in pore water pressure given by $\mu' = \mu(1 - B)$, with μ the friction coefficient and B is Skempton's coefficient, which relates pore pressure changes to normal confining stress (*King et al.*, 1994). A positive ΔCFS value indicates that faults are getting closer to shear failure; conversely, a negative

ΔCFS indicates that faults are moving away from failure. For our computations we used an effective friction coefficient of μ' = 0.35 following *Dieterich et al.* (2003). The potential slip direction was assumed to correspond to eastward motion of the spoon-shaped structure, corresponding to normal faulting at the base of the structure, and to the sinistral and dextral faults along the northern and southern branches of the main rift zone, respectively.

4. Can the evolution of normal stress changes be used to assess intrusion locations ?

4.1. The 1998-2007 period

During the March 1998 to April 2007 period, only 28% of the intrusions (seven out of 25) took place in a surface area affected by a normal stress decrease over at least 50% of its area (Figure 2 and movies in the Supplementary Materials). This indicates that, for this time period, normal stress changes are a poor predictor of intrusion location. Despite the March 1998 intrusions inducing a strong increase in normal stresses, this event does not appear to have affected the location of the 11 subsequent intrusions. For instance, the February 2000 intrusion (in magenta, in the 2000/02 plot) took place at the same location as the northern intrusion of March 1998.

More generally, 22 out of 25 intrusions took place north of the N120RZ, despite the large normal stress increase in this area which should prevent new intrusions, while only four intrusions took place south of this structure. In terms of magma volume, from 1998 to 2007, 12 Mm^3 were injected into the NERZ, while only 2 Mm^3 and 3 Mm^3 were injected into the SERZ and N120RZ, respectively (*Dumont et al.*, 2022).

The exceptions are the largest intrusive events of this period, in January 2004 and March-April 2007, to the north-east and east-south-east of the summit, respectively. The first took place in an area with marked normal stress decrease on the subhorizontal part of the spoon-shaped structure, at a location consistent with unclamping (62% negative stress values). The second took place in an area of normal stress decrease (67% of the surface), especially at its initiation point, east of the summit.

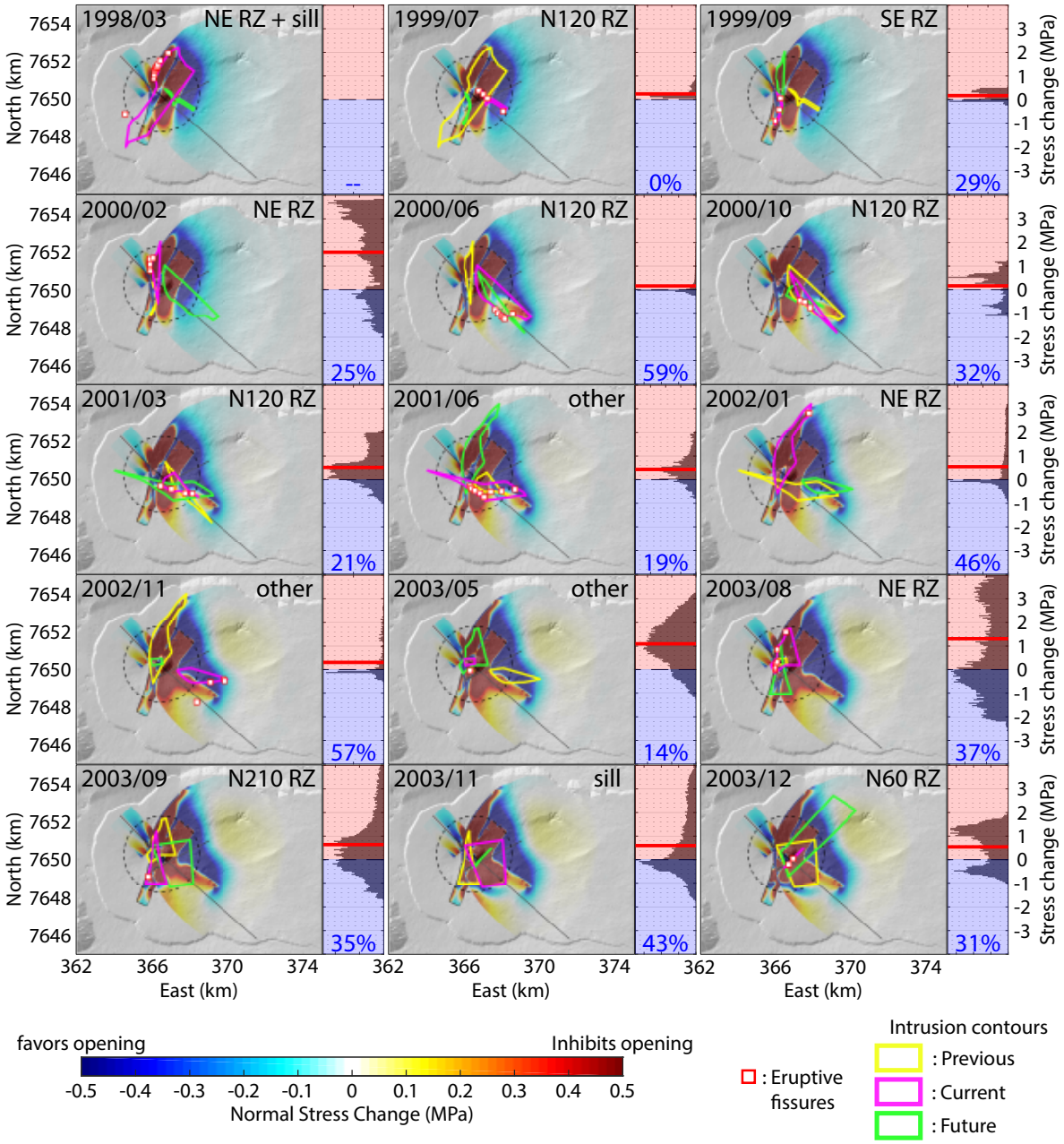

Fig. 2: Normal stress changes at Piton de la Fournaise rift zones for the 1998-2007 period. Each plot shows the cumulative normal stress change induced by previous intrusions in map view. The date of the intrusion is indicated in the top left corner (year/month), and the rift zone where the intrusion took place is indicated in the top right corner of each panel. For each date, the yellow, magenta and green contours indicate past, current and future intrusion locations, respectively. The red and white squares indicate the eruptive fissure locations. The dashed circle highlights the limit beyond which intrusions are considered to be distal (>2 km from the summit). For full 3D animated views, please refer to the Supplementary Materials. To the right side of each panel is a plot of the distribution of the cumulated normal stress changes computed for the geometry of the current intrusion, within its 95% confidence interval. The blue percentage at the bottom gives the percentage of negative values and the red line indicates the average value.

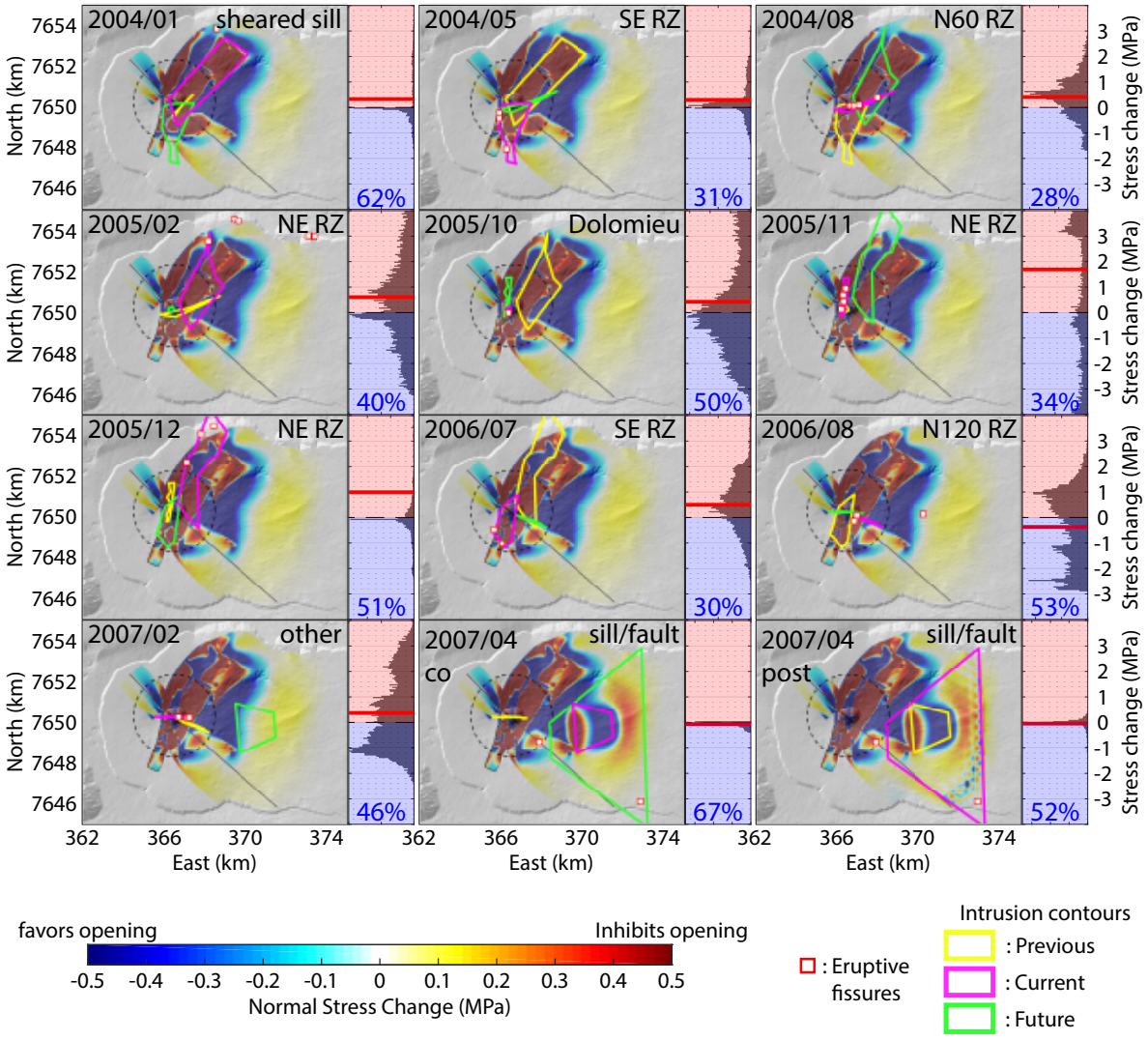

Fig. 2 (cont.)

We conclude that computed stress changes are not able to explain the observed intrusion sequence and that there is a non-uniform distribution of the intruded volumes between the north and south flank. Both observations possibly indicate a non-isotropic stress field prior to 1998.

4.2. The 2008-2021 period

For the September 2008 to October 2021 period, cumulated stress changes can predict the intrusion locations, with 44% of the intrusions (14/32) taking place along surfaces affected by normal stress decrease over at least 50% of their area (see Figure 3 and movies in the

Supplementary Materials). Moreover, regular patterns are observed with eruptions switching from one rift zone to another and, as intrusions proceed, eruptions take place further away

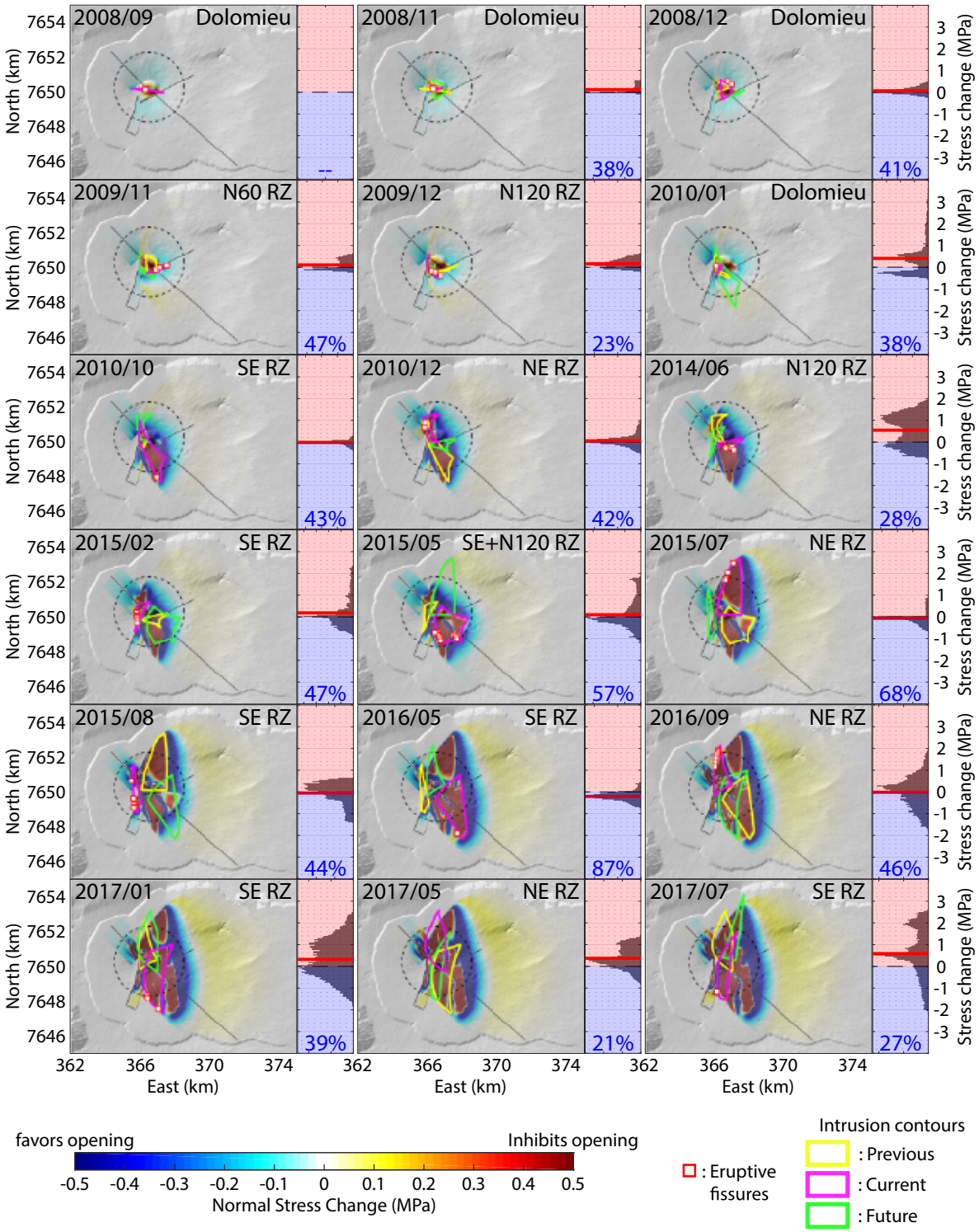

Fig. 3: Same caption as Figure 2 for the 2008 to 2021 period.

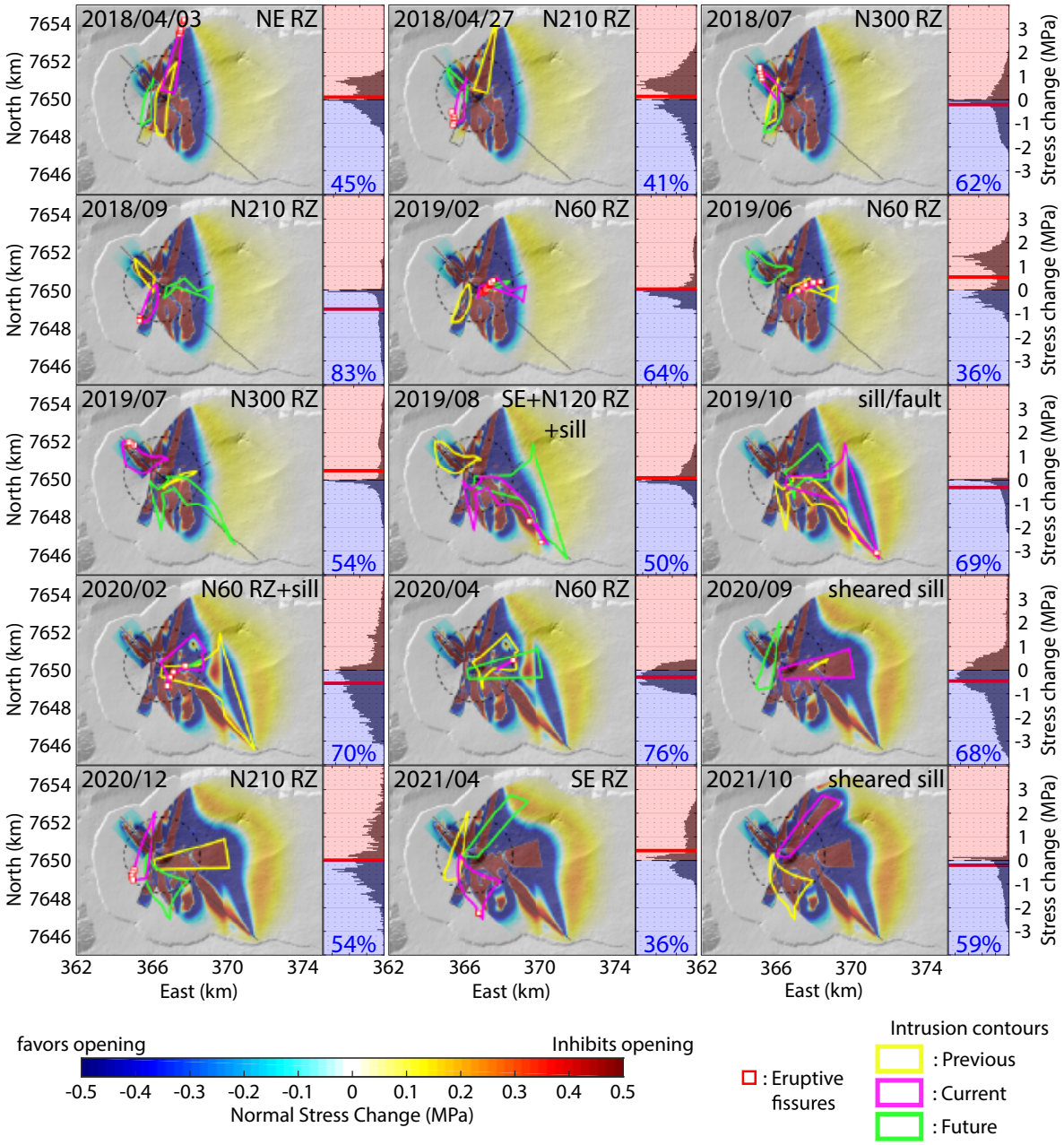

Fig. 3 (cont.)

from the summit, as well as in the sill area. Five intrusive sub-periods can be distinguished (Figure 5).

1. For the period from September 2008 until January 2010, magmatic activity is characterized by a group of six eruptions within the summit crater. Most were associated with weak deformation (< 5 cm), small intrusion volumes (< 0.3 Mm^3; *Dumont et al.*, 2022

) and hence had a low effect on the stress field, with only two showing slightly higher level of deformation (November and December 2009). There was also a large number of arrested dykes (nine according to *Roult et al.*, 2012), some of which had too little deformation to be analyzed (*Dumont et al.*, 2022).

2. Then, from October 2010 to April 2018, 12 intrusions were emplaced in the main NERZ-SERZ, with the exception of two intrusions in the N120RZ (May 2015 being in both the SERZ and the N120RZ). Intrusions alternated between the north and south flanks. Up to August 2015, six intrusions out of seven occurred in the summit and proximal areas (between 1 and 2 km from the summit). From August 2015, cumulated normal stress was highest in the proximal part of the NERZ-SERZ, indicating clamping, while negative normal stress changes occurred within the crater and the horizontal part of the main NERZ-SERZ, indicating unclamping. From May 2016 to April 2018 more frequent distal intrusions took place in the NERZ-SERZ, characterized by longer sub-horizontal intrusions at the base of the spoon shaped structure. During this period, three intrusions (January 2017, May 2017, July 2017) occurred in areas clamped by previous intrusions, but their initiation point, close to the summit, was in areas unclamped by previous intrusions. The alternation between the northern and southern flank intrusions can be explained by stress changes associated with each event, with north flank intrusions decreasing stress in the south flank and, conversely, south flank intrusions decreasing stress in the north flank (see Supplementary Figure S5 and movies), while the occurrence of more distal intrusions can be explained by cumulative stress, transferring the stress decrease further away along the rift zone.

3. After the April 4, 2018 intrusion, the whole NERZ-SERZ became clamped. The remaining unclamped areas were located beneath the eastern flank and along the secondary rift zones. From the end of April 2018 to July 2019, activity migrated to the secondary rift zones (N210RZ, the N300RZ and the N60RZ), where only two small volume intrusions had previously taken place (November and December 2009). In July

2019, these secondary rift zones showed high normal stress changes, and were also clamped, while the sill zone remained unclamped. As for the October 2010-April 2018 period, the alternation between north (N300RZ) and south (N210RZ) eruptions can be explained by cumulated stress changes.

4. From August 2019 to September 2020, the clamping in the rift zones and unclamping in the sill zone favored eastward and downward migration of the intrusive activity, which occurred as sill intrusions. Two intrusions which initially emplaced as sills turned into dykes in the N60RZ and N120RZ rift zones. The October 2019 and September 2020 sill intrusions were associated with co-eval shear displacement, inducing flank slip.

5. From December 2020 to October 2021, activity was characterized by alternations between dyke intrusions in the different rift zones and the sill zone east of the rift zones. This rapid alternation can be explained by the normal stress being sub-equal in the different rift zones as well as in the sill zone. This alternation is an indication of a prevailing critical state of stress, where normal stress is sub-equal between the different rift zones.

Throughout the 2008-2021 period, a striking feature is that the summit part of the rift zones, located beneath the crater and the sill zone, remained unclamped for geometrical reasons, as it corresponds to the tip of intrusions. This unclamping explains why intrusions could maintain the same pattern characterized by intrusions beneath the summit followed by lateral injections.

5. A positive feedback between vertical rift zone intrusions and flank slip

Previous conceptual (*Dieterich*, 1988), geophysical (*Cayol et al.*, 2000; *Walter and Amelung*, 2006; *Puglisi et al.*, 2008; *Montgomery-Brown et al.*, 2011) and geological (*Tibaldi*, 1996; *Chaput et al.*, 2014) studies have demonstrated that intrusive activity and flank slip can interact. In this section, we investigate how Piton de la Fournaise intrusive activity may change the Coulomb stress on the subhorizontal structure beneath the eastern flank, affecting flank

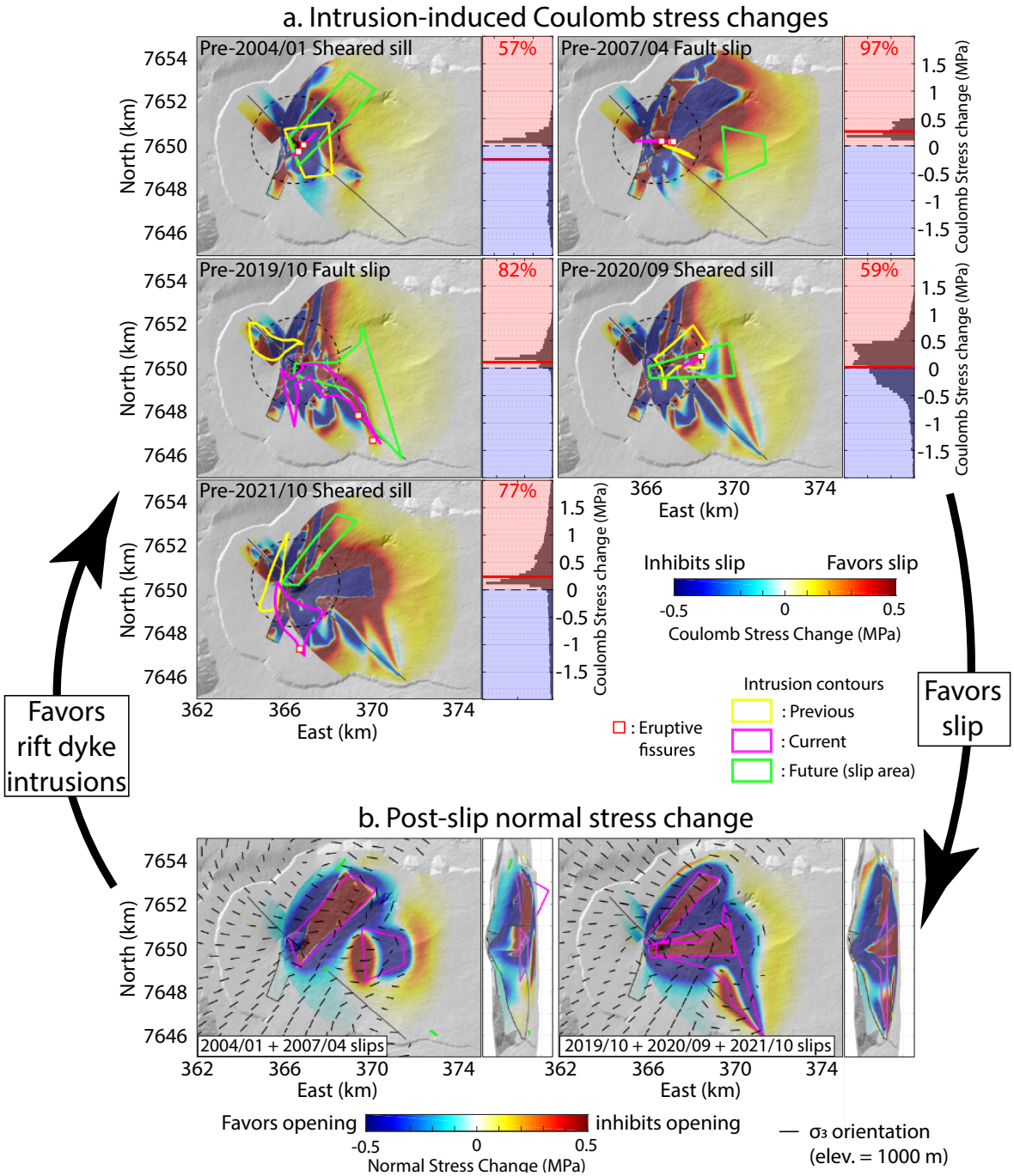

Fig. 4: Pre- and post-slip event stress changes. a. Cumulated Coulomb stress changes preceding five identified slip events for the 1998-2021 period. Coulomb stress changes are presented on the same base maps as Figures 2 and 3. The slip areas are indicated by the green contours. For full 3D animated view of Coulomb stress, see the Supplementary Materials. To the right of each panel, we indicate the distribution of the Coulomb stress change computed on the intrusion/fault geometry within its 95% confidence interval. We also indicate the percentage of positive values and the average indicated by the red line. b. Normal stress changes induced by displacement associated with the 2004/01, 2007/04, 2019/10, 2020/09 and 2021/10 slip events in map view and in north-south cross sections (showing the N120RZ and N60RZ). Black segments indicate the direction of the minimum principal stress (σ_3) at 1000 m elevation. The magenta contours indicate locations of slip events.

stability. Conversely, we investigate how flank slip events modify normal stress in the rift zones, enabling or inhibiting future intrusions.

From our previous inversion of InSAR data (*Dumont et al.*, 2022), two fault slip events were identified, in March-April 2007 and October 2019, as well as three sheared sill intrusions, in January 2004, September 2020 and October 2021. Prior to the slip events, 57-97% of the slip areas were affected by Coulomb stress increase (Figure 4a). Disregarding negative values located close to the rift zones, the average Coulomb stress increase ranges between 0.17 and 0.55 MPa. Thus, in addition to decreasing the normal stress in the eastern flank and favoring the migration of the activity towards the east (see section 4), intrusions increased the Coulomb stress in the eastern flank and promoted the occurrence of eastward slip. On the contrary, throughout the study period, the sub-vertical rift zones underwent a decrease in Coulomb stress (Figure 4a), indicating that shear failure was inhibited in the rift-zones.

We then studied how slip events modify normal stress in the rift zones, as well as on a plane located at 1000 m elevation. Figure 4b shows that the slip events relaxed the normal stresses applied to the rift zones. This stress relaxation could explain the return of activity to the rift zones in December 2020 and April 2021 after the October 2019 and September 2020 slip events. In addition to relaxing the stress, the slip events reoriented the minimum principal stress (σ_3) perpendicular to the NERZ-SERZ, ensuring the persistence of this rift zone. This supports the positive feedback between intrusions in the main NERZ-SERZ and flank slip on the subhorizonal part of the spoon-shaped structure.

6. Discussion and conclusion

The 60 intrusions that took place at Piton de la Fournaise between 1998 and 2021 can be divided into different intrusive phases corresponding to the stress field ~~, and its~~ evolution over time that differ from eruptive cycles determined by deep magma supply episodes (Figure 5). During the 1998-2007 period (phase 0 in Figure 5), we observe a lack of clear causal link between the stress evolution and the sequence of intrusions, characterized by intrusive

activity switching from one rift zone to another, irrespective of the stress evolution. Because the rate of magma supply was the same over the entire period, the minimal influence of stress evolution cannot be attributed to a higher magma pressure. However, if we assume that intrusions take place in areas of lowest normal stress, this unpredictability is indicative of an initially unknown non-isotropic stress field such that the cumulated stress changes from 1998 onward had a different pattern to the total normal stress. This inherited stress field was probably affected by higher normal stress south of the summit to explain the lack of intrusions there. This assumption is supported by the high proportion of eruptions that took place in the southern flank prior to our study. Between 1972 and 1998, 44% of eruptions took place in the south flank, 29% in the north flank and 26% in Dolomieu and the eastern flank (*Peltier et al.*, 2009).

On the other hand, after the major March-April 2007 event, we observe an agreement between the computed stress evolution and the intrusion locations. The fact that stress changes are able to predict failure, either tensile for intrusions or shear for faults and sheared intrusions, indicates that stress changes are consistent with the total stress. This implies that our start date (April 2007) for the computation cumulated stress corresponds to an isotropic stress. We chose this date because of the major events that took place in 2007 and because of the subsequent change in eruptive activity, but this predictability further justifies our hypothesis. It is likely that the 2007 flank slip, combined with the Dolomieu crater collapse relaxed the deviatoric part of the stress field. Following this "resetting" event, five different phases have been identified (Figure 5), whose sequence can be explained by cumulated normal stress from intrusions inhibiting future intrusions at the same location, and instead favoring intrusions further along the rift zones. Normal stress changes explain (1) the occurrence of increasingly distal intrusions, (2) the alternations between rift zones, and (3) the occurrence of sill intrusions. Toward the end of the study period (2021-), the normal stress is sub-equal between the different rift zones (Figure 5; phase 5). This results in a critical state of stress leading to complex alternation between the different rift zones and the sill zone.

The beginning of the 2008-2021 sequence, from September 2008 until January 2010, was characterized by summit eruptions and a high proportion of arrested dykes. The occurrence of summit eruptions contrasts with the pattern of intrusions expected after a caldera collapse (*Corbi et al.*, 2015). Indeed, *Corbi et al.* (2015) showed that, after a caldera collapse, the orientation of the minimum principal stress favors sills and circumferential dyke intrusions, provided the collapse unloading pressure Pl is five times greater than the dyke overpressure Pe. Here, we note that Pl/Pe could be less than five if the density contrast between the magma and host rocks in the collapse column was greater than 300 kg/m^3. Gravity measurements conducted after the 2007 collapse (*Gailler et al.*, 2009) indicate that such a high density contrast was indeed likely. Summit eruptions could also be encouraged by the 2007 flank slip (Figure 4), which decreased horizontal stress, and by the chaotic collapse of the rock column above the reservoir which induced a decrease in density (*Gailler et al.*, 2009) and an increase in porosity. Because porosity is inversely related to fracture toughness (*Heap and Violay*, 2021), the collapse allowed for easier magma propagation beneath the summit.

The Piton de la Fournaise cycles of intrusive activity, relative to the stress field evolution phases, differ from those at other volcanoes also characterized by rift zones activity, such as Mauna Loa (*Walter and Amelung*, 2006), Krafla (*Buck et al.*, 2006) or the Manda Hararo-Dabbahu rift (Ethiopia) (*Grandin et al.*, 2010; *Hamling et al.*, 2010). At these volcanoes, intrusive sequences start with a major intrusion followed by shorter intrusions, closer to the source. Alternations between opposite sides of a rift zone typically take place (*Walter and Amelung*, 2006; *Buck et al.*, 2006; *Grandin et al.*, 2010; *Hamling et al.*, 2010). These patterns are explained by dyke interactions (i.e. clamping at dyke locations and unclamping at dyke tips) (*Walter and Amelung*, 2006; *Hamling et al.*, 2010), and, in extensional rift settings (*Buck et al.*, 2006; *Grandin et al.*, 2010), by interactions between the regional stress and the rate of magma supply. Extensional regional stress is balanced by magma intrusions, and magma supply rate governs the distance over which magma can be transported. At Piton de la Fournaise, as for the above cited volcanoes, we observe an alternation between opposite sides

of the rift zone, but, in contrast to these volcanoes, we observe a progression from the summit to the distal zones. There is also a wider range of intrusive activity characterized by several secondary rift zones and a sill zone. These differences can be explained by the geometry of the main rift zone, which is spoon-shaped. Migration towards the distal zone is made possible by the presence of the sub-horizontal intrusion zone at depth, allowing the area clamped by previous intrusions to be bypassed from below. Such migration is unlikely to occur in purely vertical rift zones. This pattern of intrusive activity could be present at other volcanoes which also host a spoon-shaped intrusive structure. From observation of landslide deposits and fault scars, such structures could possibly be found at Mount Etna (Italy) (*Urlaub et al.*, 2018), volcanoes on the Canary islands (*Krastel et al.*, 2001), and Fogo in the Cape Verde Islands (*Barrett et al.*, 2020).

Positive feedback between sub-vertical dykes and flank slip (Figure 4) has been suggested previously by conceptual, numerical and analogue models for Hawaii (*Dieterich*, 1988; *Walter and Amelung*, 2006), Mount Etna (*Walter et al.*, 2005a), the Canary Islands (*Walter and Troll*, 2003; *Walter et al.*, 2005b) and Piton des Neiges (*Chaput et al.*, 2014). Here, we document this feedback at Piton de la Fournaise over the last two decades. Over short timescales (years to tens of years), small scale flank slip events partially unclamp the sub-vertical rift zones favoring new dyke intrusions and controlling migration of the activity. Over a longer timescale, both intrusions and slip events contribute to unclamping and increasing Coulomb stress at the tip of the spoon-shaped structure (Figure 4). If the stress accumulation is released suddenly, it may trigger a major flank collapse, generating an earthquake and a tsunami. If this event is catastrophic, it could well modify the morphology and stress state of the edifice and induce a change in the location of the volcanic center (*Maccaferri et al.*, 2017). A study by *Maccaferri et al.* (2017) shows that, because the deep magma conduit of Piton de la Fournaise is to the west of the summit crater (*Battaglia et al.*, 2005), a flank collapse would shift the volcanic center to the east. Similar flank collapses and shifts of the volcanic center may have occurred in the past, as indicated by previous volcanic centers located to the west

of the Dolomieu crater, towards the Plaine des Sables (*Letourneur et al.*, 2008; *Michon et al.*, 2015).

As indicated earlier, sporadic seismicity on the south flank aligned along a 40° dip trend is observed during magma intrusions. This could be related to the spoon-shaped structure (*Dumont et al.*, 2022). However, its dip and depth are too great to correspond to the structure we identified. An alternative hypothesis proposed by *Gerbault et al.* (2022) is that this structure corresponds to elasto-plastic strain induced by magma chamber inflation. Computations (Figure 6) show that intrusions in the main NERZ-SERZ increase Coulomb stress along 40° dip normal faults, favoring the occurrence of earthquakes. So, even if the 40° dip structure is not induced by rift intrusions, it could be activated by them. A possibility for the lack of seismic activity at the base of the spoon-shaped structure (500 m beneath the surface), and the seismicity occurring on the deeper 40° dip structure, is the difference in normal stress. At low elevations, normal stress might be too low to trigger seismicity, which might not be the case at more than 2 km depth.

This study demonstrates that stress accumulation on preexisting structures is a key parameter for anticipating short-term (years to tens of years) intrusive and flank slip activity. Forecasting intrusive activity and assessment of flank stability rely on up-to-date deformation and stress models which account for the opening of the rift-zones, as well as sheared intrusions and fault slip events on sub-horizontal structures. Using our accurate stress model with a statistical approach to magma propagation, such as the one developed by *Rivalta et al.* (2019) and *Mantiloni et al.* (2021), is a promising way to forecast intrusions and slip events.

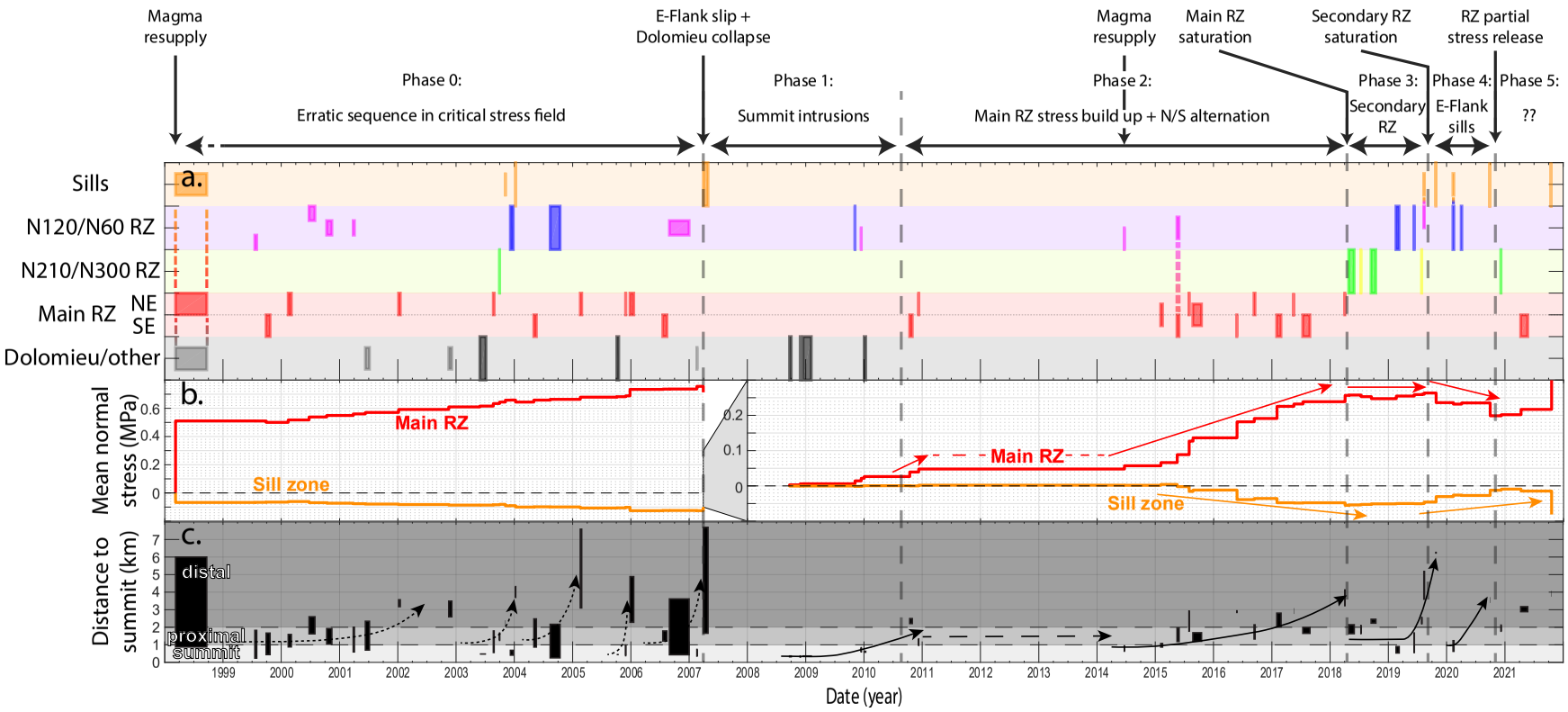

Fig. 5: 1998-2021 intrusions. a. Timeline showing each eruption as a bar color-coded for the different rift zones. Bar width indicates the eruption duration. Using the same color code as in Figure 1, eruptions within the Dolomieu are in black, eruptions in the main NERZ-SERZ are in red, eruptions in the N210RZ and N300RZ rift zone are in green and yellow, eruptions in the N120RZ and N60RZ are in magenta and blue and intrusions emplaced as sills are in light orange. Unclassified eruptions are in light gray. For the main NERZ-SERZ, the vertical position of the bar also indicates SE (bottom) and NE (top) intrusions. Note that March 1998, May 2015 and February 2020 eruptions overlap several rift zones. b. Normal stress change averaged across the main NERZ-SERZ and the sill zone. Note the change of the scale between the 1998-2007 and 2008-2021 periods for clarity. c. Distance from the summit between the start and end points of the eruptive fissures for each intrusion. The shade of gray of the background indicates the boundaries between summit (< 1 km from the summit, light gray), proximal (between 1 and 2 km from the summit, medium gray) and distal (>2 km from the summit, dark gray) eruptions. Dashed black arrows indicate distance evolution reported by *Peltier et al.* (2009), and solid black arrows indicate the general trend determined in the present study.

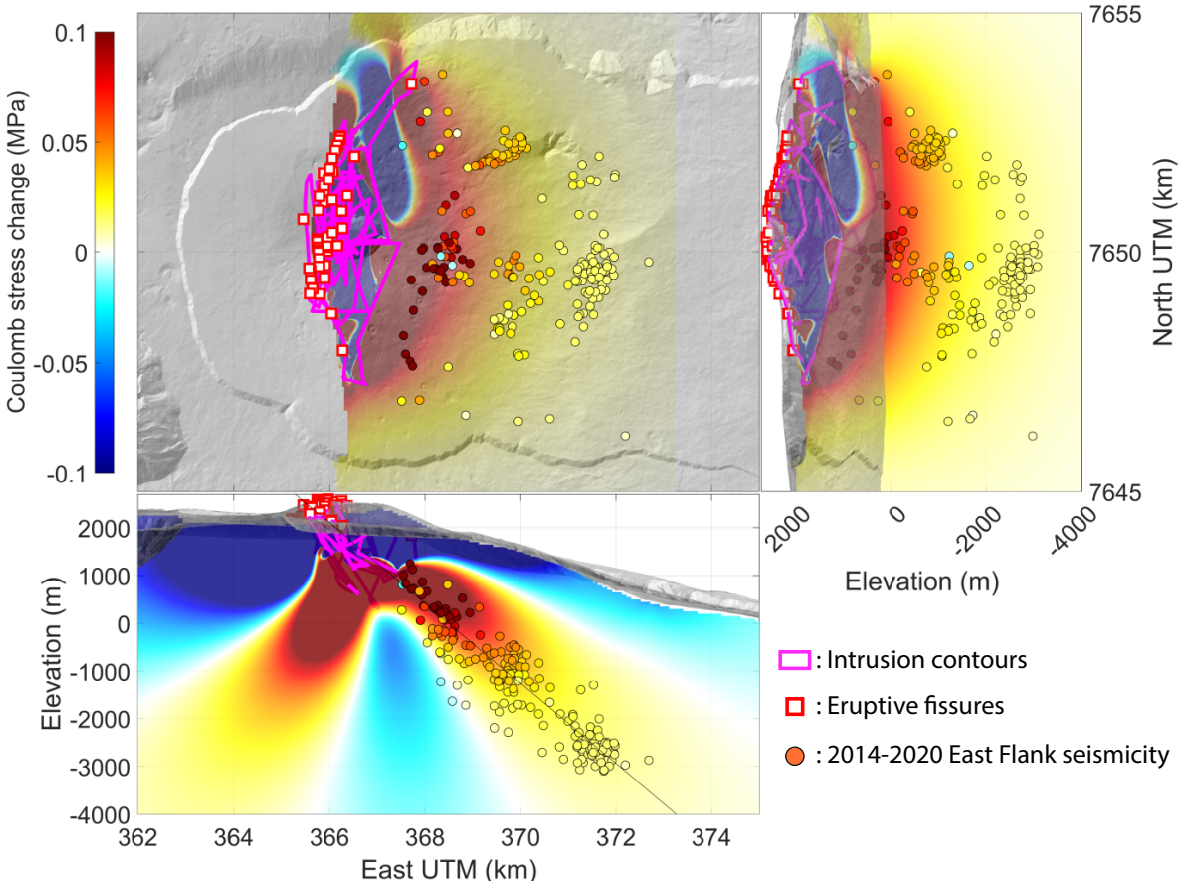

Fig. 6: Coulomb stress change on the East Flank seismic plane. Coulomb stress was calculated from intrusions occurring in the vertical part of the main NERZ-SERZ (2000/02, 2002/01, 2003/08, 2003/09, 2004/05, 2005/11, 2006/07, 2010/12, 2015/02, 2015/08, 2016/09), by assuming eastward normal faults inclined at 40°. The circles indicate seismic hypocenters. East-West cross-section shows a vertical profile whose location is indicated by a dashed line on the map view. Map view and North-South views show slices passing through the seismic plane as indicated by the solid line in the East-West cross-section.

Credit authorship contribution statement

Quentin Dumont: Conceptualization, Methodology, Analysis, Validation, Visualization, Writing original draft, Review & Editing.

Valérie Cayol: Provided the numerical codes for the stress computation, Validation, Writing original draft, Review & Editing.

Jean-Luc Froger: Validation, Writing, Review & Editing.

Declaration of competing interest

The authors declare that they have no known competing financial interests or personal relationships that could have appeared to influence the work reported in this paper.

Acknowledgements

This work was supported by the TelluS program of CNRS/INSU, by the EUROVOLC project, under the EU Horizon 2020 Research and Innovation Action, grant No. 731070. InSAR data were acquired within the framework of the Indian Ocean InSAR Observatory (OI^2/ISDeform/INSU). We thank Eleonora Rivalta and Lorenzo Mantiloni for usefull discusions. We also thank Fran van Wyk de Vries for proofreading the english of the manuscript. We thank JAXA and INTA for providing the ALOS-2 and PAZ data respectively, through the 4 th ALOS RA #1287 project and the PAZ AO-001-024 project. Deformation modelling benefited from the infrastructure and assistance of the Mésocentre from the University of Clermont Auvergne, from funds from French Government Laboratory of Excellence initiative no. ANR-10-LABX-0006. This is a Laboratory of Excellence Clervolc contribution number xxx.

References

Albino, F., V. Pinel, and F. Sigmundsson (2010), Influence of surface load variations on eruption likelihood: Application to two Icelandic subglacial volcanoes, Grímsvötn

and Katla, *Geophysical Journal International*, *181*(3), 1510–1524, doi:10.1111/j.1365-246X.2010.04603.x.

Amelung, F., S. H. Yun, T. R. Walter, P. Segall, and S. W. Kim (2007), Stress control of deep rift intrusion at Mauna Loa volcano, Hawaii, *Science*, *316*(5827), 1026–1030, doi:10.1126/science.1140035.

Anderson, E. (1951), *The Dynamics of Faulting and Dyke Formation with Applications to Britain*, Oliver and Boyd, Edinburgh.

Auker, M. R., R. S. J. Sparks, L. Siebert, H. S. Crosweller, and J. Ewert (2013), A statistical analysis of the global historical volcanic fatalities record, *Journal of Applied Volcanology*, *2*(1), 1–24, doi:10.1186/2191-5040-2-2.

Barrett, R., E. Lebas, R. Ramalho, I. Klaucke, S. Kutterolf, A. Klügel, K. Lindhorst, F. Gross, and S. Krastel (2020), Revisiting the tsunamigenic volcanic flank collapse of Fogo Island in the Cape Verdes, offshore West Africa, *Geological Society, London, Special Publications*.

Battaglia, J., V. Ferrazzini, T. Staudacher, K. Aki, and J. L. Cheminée (2005), Pre-eruptive migration of earthquakes at the Piton de la Fournaise volcano (Réunion Island), *Geophysical Journal International*, *161*(2), 549–558, doi:10.1111/j.1365-246X.2005.02606.x.

Beauducel, F., A. Peltier, A. Villié, and W. Suryanto (2020), Mechanical Imaging of a Volcano Plumbing System From GNSS Unsupervised Modeling, *Geophysical Research Letters*, *47*(17), doi:10.1029/2020GL089419.

Buck, W. R., P. Einarsson, and B. Brandsdóttir (2006), Tectonic stress and magma chamber size as controls on dike propagation: Constraints from the 1975-1984 Krafla rifting episode, *Journal of Geophysical Research: Solid Earth*, *111*(12), 1–15, doi:10.1029/2005JB003879.

Cayol, V., and F. H. Cornet (1997), 3D mixed boundary elements for elastostatic deformation field analysis, *International journal of rock mechanics and mining ...*, *34*(2), 275–287, doi:10.1016/S0148-9062(96)00035-6.

Cayol, V., and F. H. Cornet (1998), Three-dimensional modeling of the 1983–1984 eruption at Piton de la Fournaise Volcano, Réunion Island, *Journal of Geophysical Research*, *103*(B8), 18,025, doi:10.1029/98JB00201.

Cayol, V., J. H. Dieterich, A. T. Okamura, and A. Miklius (2000), High magma storage rates before the 1983 eruption of Kilauea, Hawaii, *Science*, *288*(5475), 2343–2346, doi: 10.1126/science.288.5475.2343.

Chadwick, W. W., and J. H. Dieterich (1995), Mechanical modeling of circumferential and radial dike intrusion on Galapagos volcanoes, *Journal of Volcanology and Geothermal Research*, *66*(1-4), 37–52, doi:10.1016/0377-0273(94)00060-T.

Chaput, M., V. Famin, and L. Michon (2014), Deformation of basaltic shield volcanoes under cointrusive stress permutations, *Journal of Geophysical Research: Solid Earth*, *119*(1), 274–301, doi:10.1002/2013JB010623.

Chen, Y., D. Remy, J. L. Froger, A. Peltier, N. Villeneuve, J. Darrozes, H. Perfettini, and S. Bonvalot (2017), Long-term ground displacement observations using InSAR and GNSS at Piton de la Fournaise volcano between 2009 and 2014, *Remote Sensing of Environment*, *194*(March 1998), 230–247, doi:10.1016/j.rse.2017.03.038.

Chevrel, M. O., M. Favalli, N. Villeneuve, A. J. Harris, A. Fornaciai, N. Richter, A. Derrien, P. Boissier, A. DI Muro, and A. Peltier (2021), Lava flow hazard map of Piton de la Fournaise volcano, *Natural Hazards and Earth System Sciences*, *21*(8), 2355–2377, doi: 10.5194/nhess-21-2355-2021.

Corbi, F., E. Rivalta, V. Pinel, F. Maccaferri, M. Bagnardi, and V. Acocella (2015), How

caldera collapse shapes the shallow emplacement and transfer of magma in active volcanoes, *Earth and Planetary Science Letters*, *431*, 287–293, doi:10.1016/j.epsl.2015.09.028.

Dieterich, J. H. (1988), Growth and Persistence of Hawaiian Volcanic Rift Zones, *Journal of Geophysical Research*, *93*, 4258–4270, doi:10.1029/JB093iB05p04258.

Dieterich, J. H., V. Cayol, and P. Okubo (2003), Stress Changes Before and During the Pu'u 'O'o Kupaianaha Eruption, *US Geological Survey Professional Paper*, *1676*, 187.

Dumont, Q., V. Cayol, J. Froger, and A. Peltier (2022), 22 years of satellite imagery reveal a major destabilization structure at Piton de la Fournaise, *Nature communications*, *13*, 1–11, doi:10.1038/s41467-022-30109-w.

Duputel, Z., V. Ferrazzini, O. Lengliné, L. Michon, F. R. Fontaine, and F. Massin (2021), Seismicity of La Réunion island, *Comptes Rendus Géosciences*, pp. 0–19.

Froger, J. L., V. Famin, V. Cayol, A. Augier, L. Michon, and J. F. Lénat (2015), Time-dependent displacements during and after the April 2007 eruption of Piton de la Fournaise, revealed by interferometric data, *Journal of Volcanology and Geothermal Research*, *296*(April 2007), 55–68, doi:10.1016/j.jvolgeores.2015.02.014.

Fukushima, Y., V. Cayol, and P. Durand (2005), Finding realistic dike models from interferometric synthetic aperture radar data: The February 2000 eruption at Piton de la Fournaise, *Journal of Geophysical Research B: Solid Earth*, *110*(3), 1–15, doi:10.1029/2004JB003268.

Gailler, L. S., J. F. Lénat, M. Lambert, G. Levieux, N. Villeneuve, and J. L. Froger (2009), Gravity structure of Piton de la Fournaise volcano and inferred mass transfer during the 2007 crisis, *Journal of Volcanology and Geothermal Research*, *184*(1-2), 31–48, doi:10.1016/j.jvolgeores.2009.01.024.

Gerbault, M., F. J. Fontaine, A. Peltier, J. L. Got, R. Hassani, V. Ferrazzini, L. Gailler, and Z. Duputel (2022), What causes the persistent seismicity below the eastern flank

of Piton de la Fournaise (la Réunion Island)? Elasto-plastic models of magma inflation, *Journal of Volcanology and Geothermal Research*, *431*(March), 107,628, doi: 10.1016/j.jvolgeores.2022.107628.

Grandin, R., A. Socquet, E. Jacques, N. Mazzoni, J. B. De Chabalier, and G. C. King (2010), Sequence of rifting in Afar, Manda-Hararo rift, Ethiopia, 2005-2009: Time-space evolution and interactions between dikes from interferometric synthetic aperture radar and static stress change modeling, *Journal of Geophysical Research: Solid Earth*, *115*(10), 2005–2009, doi:10.1029/2009JB000815.

Gudmundsson, A. (2012), Magma chambers: Formation, local stresses, excess pressures, and compartments, *Journal of Volcanology and Geothermal Research*, *237-238*, 19–41, doi:10.1016/j.jvolgeores.2012.05.015.

Hamling, I. J., T. J. Wright, E. Calais, L. Bennati, and E. Lewi (2010), Stress transfer between thirteen successive dyke intrusions in Ethiopia, *Nature Geoscience*, *3*(10), 713–717, doi: 10.1038/ngeo967.

Heap, M. J., and M. E. Violay (2021), The mechanical behaviour and failure modes of volcanic rocks: a review, *Bulletin of Volcanology*, *83*(5), doi:10.1007/s00445-021-01447-2.

Heap, M. J., M. Villeneuve, F. Albino, J. I. Farquharson, E. Brothelande, F. Amelung, J. L. Got, and P. Baud (2020), Towards more realistic values of elastic moduli for volcano modelling, *Journal of Volcanology and Geothermal Research*, *390*, 106,684, doi: 10.1016/j.jvolgeores.2019.106684.

Hrysiewicz, A. (2019), Caractérisation des déplacements liés aux coulées de lave au Piton de la Fournaise à partir de données InSAR, Ph.D. thesis, Université Clermont Auvergne.

Kelfoun, K., T. Giachetti, and P. Labazuy (2010), Landslide-generated tsunamis at Réunion Island, *Journal of Geophysical Research: Earth Surface*, *115*(4), 1–17, doi: 10.1029/2009JF001381.

King, G. C. P., R. S. Stein, and J. Lin (1994), Static stress changes and the triggering of earthquakes, *Bulletin of the sismological Society of America*, *84*(3), 935, doi:10.1016/0148-9062(95)94484-2.

Krastel, S., H.-U. Schmincke, C. L. Jacobs, R. Rihm, T. P. Le Bas, and B. Alibés (2001), Submarine landslides around the Canary Islands, *Journal of Geophysical Research*, *106*, 3977–3997.

Le Corvec, N., and P. J. McGovern (2018), The Effect of Ocean Loading on the Growth of Basaltic Ocean Island Volcanoes and Their Magmatic Plumbing System, *Frontiers in Earth Science*, *6*(September), doi:10.3389/feart.2018.00119.

Lengliné, O., Z. Duputel, and V. Ferrazzini (2016), Uncovering the hidden signature of a magmatic recharge at Piton de la Fournaise volcano using small earthquakes, *Geophysical Research Letters*, *43*(9), 4255–4262, doi:10.1002/2016GL068383.

Letourneur, L., A. Peltier, T. Staudacher, and A. Gudmundsson (2008), The effects of rock heterogeneities on dyke paths and asymmetric ground deformation: The example of Piton de la Fournaise (Réunion Island), *Journal of Volcanology and Geothermal Research*, *173*(3-4), 289–302, doi:10.1016/j.jvolgeores.2008.01.018.

Lin, G., and P. G. Okubo (2020), Seismic Evidence for a Shallow Detachment Beneath Kīlauea's South Flank During the 2018 Activity, *Geophysical Research Letters*, *47*(15), 1–20, doi:10.1029/2020gl088003.

Maccaferri, F., M. Bonafede, and E. Rivalta (2011), A quantitative study of the mechanisms governing dike propagation, dike arrest and sill formation, *Journal of Volcanology and Geothermal Research*, *208*(1-2), 39–50, doi:10.1016/j.jvolgeores.2011.09.001.

Maccaferri, F., N. Richter, and T. R. Walter (2017), The effect of giant lateral collapses on magma pathways and the location of volcanism, *Nature Communications*, *8*(1), 1–11, doi:10.1038/s41467-017-01256-2.

Mantiloni, L., T. Davis, A. B. Gaete Rojas, and E. Rivalta (2021), Stress Inversion in a Gelatin Box: Testing Eruptive Vent Location Forecasts With Analog Models, *Geophysical Research Letters*, *48*(6), 1–11, doi:10.1029/2020GL090407.

Menand, T., K. A. Daniels, and P. Benghiat (2010), Dyke propagation and sill formation in a compressive tectonic environment, *Journal of Geophysical Research: Solid Earth*, *115*(8), doi:10.1029/2009JB006791.

Michon, L., V. Ferrazzini, A. Di Muro, N. Villeneuve, and V. Famin (2015), Rift zones and magma plumbing system of Piton de la Fournaise volcano: How do they differ from Hawaii and Etna?, *Journal of Volcanology and Geothermal Research*, *303*, 112–129, doi:10.1016/j.jvolgeores.2015.07.031.

Montgomery-Brown, E. K., D. K. Sinnett, K. M. Larson, M. P. Poland, P. Segall, and A. Miklius (2011), Spatiotemporal evolution of dike opening and décollement slip at Kilauea Volcano, Hawai'i, *Journal of Geophysical Research: Solid Earth*, *116*(3), 1–14, doi:10.1029/2010JB007762.

Montgomery-Brown, E. K., M. P. Poland, and A. Miklius (2015), *Delicate Balance of Magmatic-Tectonic Interaction at Kilauea Volcano, Hawai'i, Revealed from Slow Slip Events*, 269–288 pp., Geophysical Monograph 208.

Oehler, J. F., J. F. Lénat, and P. Labazuy (2008), Growth and collapse of the Reunion Island volcanoes, *Bulletin of Volcanology*, *70*(6), 717–742, doi:10.1007/s00445-007-0163-0.

Owen, S. E., and R. Bürgmann (2006), An increment of volcano collapse: Kinematics of the 1975 Kalapana, Hawaii, earthquake, *Journal of Volcanology and Geothermal Research*, *150*(1-3), 163–185, doi:10.1016/j.jvolgeores.2005.07.012.

Peltier, A., V. Ferrazzini, T. Staudacher, and P. Bachèlery (2005), Imaging the dynamics of dyke propagation prior to the 2000-2003 flank eruptions at Piton de la Fournaise, Reunion Island, *Geophysical Research Letters*, *32*(22), 1–5, doi:10.1029/2005GL023720.

Peltier, A., V. Famin, P. Bachèlery, V. Cayol, Y. Fukushima, and T. Staudacher (2008), Cyclic magma storages and transfers at Piton de La Fournaise volcano (La Réunion hotspot) inferred from deformation and geochemical data, *Earth and Planetary Science Letters*, *270*(3-4), 180–188, doi:10.1016/j.epsl.2008.02.042.

Peltier, A., P. Bachèlery, and T. Staudacher (2009), Magma transport and storage at Piton de La Fournaise (La Réunion) between 1972 and 2007: A review of geophysical and geochemical data, *Journal of Volcanology and Geothermal Research*, *184*(1-2), 93–108, doi:10.1016/j.jvolgeores.2008.12.008.

Peltier, A., T. Staudacher, and P. Bachèlery (2010), New behaviour of the Piton de La Fournaise volcano feeding system (La Réunion Island) deduced from GPS data: Influence of the 2007 Dolomieu caldera collapse, *Journal of Volcanology and Geothermal Research*, *192*(1-2), 48–56, doi:10.1016/j.jvolgeores.2010.02.007.

Peltier, A., J.-l. Got, N. Villeneuve, P. Boissier, T. Staudacher, V. Ferrazzini, and A. Walpersdorf (2015a), Long-term mass transfer at Piton de la Fournaise volcano evidenced by strain distribution derived from GNSS network, *Journal of Geophysical Research: Solid Earth*, *120*, 1874–1889, doi:10.1002/2014JB011738.

Peltier, A., M. P. Poland, and T. Staudacher (2015b), Are Piton de la Fournaise (La Réunion) and Kilauea (Hawai'i) Really "Analog Volcanoes"?, *American Geophysical Union Monograph*, *208*, 507–531, doi:10.1002/9781118872079.ch23.

Pezzo, G., M. Palano, C. Tolomei, P. De Gori, S. Calcaterra, P. Gambino, and C. Chiarabba (2020), Flank sliding: A valve and a sentinel for paroxysmal eruptions and magma ascent at Mount Etna, Italy, *Geology*, *48*(11), 1077–1082, doi:10.1130/g47656.1.

Pinel, V., and C. Jaupart (2000), The effect of edifice load on magma ascent beneath a volcano, *Philosophical Transactions of the Royal Society A: Mathematical, Physical and Engineering Sciences*, *358*(1770), 1515–1532, doi:10.1098/rsta.2000.0601.

Puglisi, G., A. Bonforte, A. Ferretti, F. Guglielmino, M. Palano, and C. Prati (2008), Dynamics of Mount Etna before, during, and after the July-August 2001 eruption inferred from GPS and differential synthetic aperture radar interferometry data, *Journal of Geophysical Research: Solid Earth*, *113*(6), 1–20, doi:10.1029/2006JB004811.

Rivalta, E., B. Taisne, A. P. Bunger, and R. F. Katz (2015), A review of mechanical models of dike propagation: Schools of thought, results and future directions, *Tectonophysics*, *638*(C), 1–42, doi:10.1016/j.tecto.2014.10.003.

Rivalta, E., F. Corbi, L. Passarelli, V. Acocella, T. Davis, and M. A. Di Vito (2019), Stress inversions to forecast magma pathways and eruptive vent location, *Science Advances*, *5*(7), 1–12, doi:10.1126/sciadv.aau9784.

Roult, G., A. Peltier, B. Taisne, T. Staudacher, V. Ferrazzini, and A. Di Muro (2012), A new comprehensive classification of the Piton de la Fournaise activity spanning the 1985-2010 period. Search and analysis of short-term precursors from a broad-band seismological station, *Journal of Volcanology and Geothermal Research*, *241-242*, 78–104, doi:10.1016/j.jvolgeores.2012.06.012.

Ruch, J., T. Wang, W. Xu, M. Hensch, and S. Jónsson (2016), Oblique rift opening revealed by reoccurring magma injection in central Iceland, *Nature Communications*, *7*(September), doi:10.1038/ncomms12352.

Sigmundsson, F., A. Hooper, S. Hreinsdóttir, K. S. Vogfjörd, B. G. Ófeigsson, E. R. Heimisson, S. Dumont, M. Parks, K. Spaans, G. B. Gudmundsson, V. Drouin, T. Árnadóttir, K. Jónsdóttir, M. T. Gudmundsson, T. Högnadóttir, H. M. Fridriksdóttir, M. Hensch, P. Einarsson, E. Magnússon, S. Samsonov, B. Brandsdóttir, R. S. White, T. Ágústsdóttir, T. Greenfield, R. G. Green, Á. R. Hjartardóttir, R. Pedersen, R. A. Bennett, H. Geirsson, P. C. la Femina, H. Björnsson, F. Pálsson, E. Sturkell, C. J. Bean, M. Möllhoff, A. K. Braiden, and E. P. Eibl (2015), Segmented lateral dyke growth in a rifting event at Bardarbunga volcanic system, Iceland, *Nature*, *517*(7533), doi:10.1038/nature14111.

Smittarello, D., V. Cayol, V. Pinel, A. Peltier, J.-L. Froger, and V. Ferrazzini (2019), Magma Propagation at Piton de la Fournaise From Joint Inversion of InSAR and GNSS, *Journal of Geophysical Research: Solid Earth*, *124*(2), 1361–1387, doi:10.1029/2018JB016856.

Staudacher, T., V. Ferrazzini, A. Peltier, P. Kowalski, P. Boissier, P. Catherine, F. Lauret, and F. Massin (2009), The April 2007 eruption and the Dolomieu crater collapse, two major events at Piton de la Fournaise (La Réunion Island, Indian Ocean), *Journal of Volcanology and Geothermal Research*, *184*(1-2), 126–137, doi:10.1016/j.jvolgeores.2008.11.005.

Tibaldi, A. (1996), Mutual influence of dyking and collapses at Stromboli volcano, Italy, *Geological Society, London, Special Publications*, *110*, 55–63, doi: 10.1144/GSL.SP.1996.110.01.04.

Urlaub, M., F. Petersen, F. Gross, A. Bonforte, G. Puglisi, F. Guglielmino, S. Krastel, D. Lange, and H. Kopp (2018), Gravitational collapse of Mount Etna's southeastern flank, *Science Advances*, *4*(10), 1–8, doi:10.1126/sciadv.aat9700.

Villeneuve, N., and P. Bachelery (2006), Revue de la typologie des éruptions au Piton de la Fournaise, processus et risques volcaniques associés, *CyberGeo*, pp. 1–25, doi: 10.4000/cybergeo.2536.

Vlastélic, I., A. Di Muro, P. Bachèlery, L. Gurioli, D. Auclair, and A. Gannoun (2018), Control of source fertility on the eruptive activity of Piton de la Fournaise volcano, La Réunion, *Scientific Reports*, *8*(1), 1–7, doi:10.1038/s41598-018-32809-0.

Walter, T. R., and F. Amelung (2006), Volcano-earthquake interaction at Mauna Loa volcano, Hawaii, *Journal of Geophysical Research: Solid Earth*, *111*(5), 1–17, doi: 10.1029/2005JB003861.

Walter, T. R., and V. R. Troll (2003), Experiments on rift zone evolution in unstable volcanic edifices, *Journal of Volcanology and Geothermal Research*, *127*, 107–120, doi: 10.1016/S0377-0273(03)00181-1.

Walter, T. R., V. Acocella, M. Neri, and F. Amelung (2005a), Feedback processes between magmatic events and flank movement at Mount Etna (Italy) during the 2002 – 2003 eruption, *Journal of Geophysical Research*, *110*, 1–12, doi:10.1029/2005JB003688.

Walter, T. R., V. R. Troll, B. Cailleau, A. Belousov, H. U. Schmincke, F. Amelung, and P. Bogaard (2005b), Rift zone reorganization through flank instability in ocean island volcanoes: An example from Tenerife, Canary Islands, *Bulletin of Volcanology*, *67*(4), 281–291, doi: 10.1007/s00445-004-0352-z.